Improved RANS methodology to account for flow separation on rough blades

Gutiérrez, R.; Aranguren, P.; Zamponi, R.

DOI
10.1088/1742-6596/2767/2/022002

Publication date
2024

Document Version
Final published version

Published in
Journal of Physics: Conference Series

Journal of Physics: Conference Series

Improved RANS methodology to account for flow separation on rough blades

To cite this article: R Gutiérrez *et al* 2024 *J. Phys.: Conf. Ser.* **2767** 022002

Improved RANS methodology to account for flow separation on rough blades

R Gutiérrez[1], **P Aranguren**[2], **R Zamponi**[3,4]

[1]Nordex SE, Avenida Ciudad de la Innovación 3, 31621 Sarriguren, Navarra, Spain.
[2]Engineering Department, Public University of Navarre, Pamplona, Spain.
[3]Department of Environmental and Applied Fluid Dynamics, von Karman Institute for Fluid Dynamics, Sint-Genesius-Rode, Belgium
[4]Department of Flow Physics and Technology, Faculty of Aerospace Engineering, Delft University of Technology, Delft, The Netherlands

E-mail: `RGutierrez@nordex-online.com`

Abstract. The RANS inaccuracy in predicting flow separation becomes relevant in thick-modern blades, especially once they get dirt or eroded. The literature has tackled the problem by modifying the coefficient a_1 in the $k - \omega - SST$ turbulence model without considering its dependency on the adverse pressure gradient condition. This study aims to assess the mentioned dependency by estimating a_1 per blade side and angle of attack. Pressure-coefficient measurements for 18 %, 25 %, and 30 % thick airfoils in clean-inflow conditions at a Reynolds number based on chord of 3×10^6 are considered in the estimation. Hence, a unique variation of a_1 is obtained per each airfoil, justifying the need to adapt a_1 locally within the OpenFOAM code. This modification considerably improves the flow separation prediction with respect to the standard a_1 value and the f_b method. As a result, the C_L error is reduced by 8 %, whereas a certain C_D error remains for all the RANS solutions. Finally, an aeroelastic model of a 4.5 MW wind turbine reveals that the non-corrected RANS solution causes an overshoot of power and loads near rated power, whereas the corrected RANS replicates the shape of the power and loads curves. Consequently, the suggested methodology can be used to search for the required a_1 relation to local flow conditions.

1. Introduction

Two-dimensional Reynolds-average Navier-Stokes (RANS) calculations and the blade element momentum (BEM) theory remain the most affordable combination to design blades and extract boundary layer (BL) properties for noise estimations or add-ons sizing [1]. However, RANS approach lacks accuracy in predicting flow separation, which becomes relevant on modern-thick blades. Their high adverse pressure gradient (APG) enhances flow separation, especially for leading-edge roughness (LER) conditions, i.e: eroded or dirt blades. Hence, the mentioned methodology lacks reliability to judge the blade-design robustness on the surface condition.

Historically, the RANS accuracy on flow separation has been improved by lowering the eddy-viscosity within the BL. Studies [5, 6] based on the $k - \omega - SST$ turbulence model reduced the Bradshaw's coefficient a_1 from its default value of 0.31, which was derived from zero pressure gradient flows. Additionally, this coefficient is applied equally to the entire airfoil and controls the turbulent shear stress level within the BL and, in turn, the eddy viscosity. Nevertheless, Simpson *et al.* [7] indicated that a_1 varies inversely with the local APG condition and remains below 0.31. For an airfoil, a specific APG condition is defined for each side and angle of attack (AoA). As a consequence, the literature methodology may lack accuracy since, even reducing the a_1 value below 0.31, the same value is used on both airfoil sides and for any AoA. Bangga *et al.* [8] suggested an alternative method to reduce the eddy viscosity locally. Their method, denoted in this study as the f_b method, activates a damping factor f_b near the flow separation region. This factor was demonstrated to work suitably under clean conditions for different airfoils. However, the unique validation of this method under LER conditions was provided by Gutierrez *et al.* [9] in which a_1 was also demonstrated to vary and remain around 0.29. However, the conclusions were drawn under specific APG conditions and further validation is required because the understanding of a_1 dependency with the APG condition is essential to develop suitable numerical predictions.

Thus, this study aims to extend the work in [9] after estimating the a_1 value per airfoil side and AoA to consider its dependency on the APG and LER conditions of a wind turbine blade. As a result, a new methodology is suggested in Section 2.4 and the resulting aerodynamic coefficient prediction is compared with the one of the f_b method in Section 3.2. Finally, a wind turbine, based on industrial needs, is selected for aero-elastic calculations to quantify the prediction accuracy of the wind turbine performance, as shown in Section 3.3.

2. Methodology

2.1. Wind-turbine description

A 4.5 MW pith-controlled horizontal-axis wind turbine was chosen for this study with a blade length (L) of 75.8 m and a hub height of 120 m. As a result, the rotor diameter is 155 m with cone and tilt angles of 5°. The wind-turbine is in an up-wind configuration and corresponds to an IEC class S, being the cut-in and cut-out wind speeds of $3\,\mathrm{m\,s^{-1}}$ and $25\,\mathrm{m\,s^{-1}}$, respectively.

The chosen reference wind turbine was used in a complementary study [3] in which different blade designs were generated via the interpolation of two thickness distributions. The interpolation factor was denoted as F and a value of 0.5 is selected which is in line with the literature statements [24, 25] that modern blades tend to be relatively thicker in their outer part than old blades. As a result, the integration of the t/c blade distribution from 50 %L to the tip reveals an increase of the selected blade of 42 % and 6.5 % with respect to NREL5MW [19] and IWES7.5MW [20] reference wind turbines, respectively.

2.2. Calculation of wind-turbine performance and loads

The software DNV-GL Bladed [11] was used to calculate the wind turbine energy yield and loads. In this regard, the blade is defined by 61 cross-sections whose structural properties were estimated for a two-shear web configuration using the software PreComp v1.0 from NREL [10]. Additionally, the blade was assumed to be composed of different glass-fiber fabrics along with core materials infused in a matrix of epoxy resin.

Similarly to NREL 5MW reference wind turbine [19] the aerodynamic data, C_L, C_D, C_M vs. AoA, along the blade was only specified for specific cross-sections which are referred to as master airfoils. For intermediate airfoils, the aerodynamic data were linearly interpolated with respect to the t/c of adjacent master airfoils. Due to the available data, master airfoils were specified for t/c values of 40 %, 35 %, 30 %, 25 %, and 18 %.

IOP Publishing
doi:10.1088/1742-6596/2767/2/022002

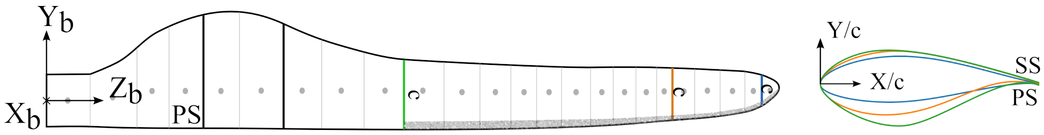

Figure 1: Illustration of the blade discretization to perform BEM calculations. LER extension along the blade length is shown in a shadow region. The reference system of the blade is marked by b, whereas the local reference system of the airfoils is normalized by their chord length c.

The LER region was defined from the 50 % of the blade length to the blade tip which covers the 30 %, 25 %, and 18 % master airfoils as shown in Figure 1. As it has been followed in a similar study [6], a Reynolds number based on chord length (Re_c) of 3×10^6 was assumed along the blade due to the availability of experimental data. The experimental data of the 30 % was obtained in the Low-Speed Low-Turbulence Wind Tunnel of TU-Delft and was presented in [16]. On the other hand 25 % and 18 % thick airfoils were tested in the DNW-HDG High Pressure Wind Tunnel in Göttingen (HDG) by Llorente *et al.* [17]. Regarding the LER-experimental setup, the first 8 % of the chord length (c) on both airfoil sides was covered for all the airfoils. However, sandpaper P100 was used for the 30 % thick airfoil while carborundum grains P60 were blown for the other two airfoils, resulting in a non-dimensional grain height (k_g/c) of 2.7×10^{-4} and 4.67×10^{-4}, respectively.

Steady calculations were performed in Bladed with uniform steady winds which were independent from each other for each wind speed. Thus, the deflections of the flexible blade components do not vary in time. Regarding the control scheme, a variable speed and pitch feathering configuration was chosen with independence from previous wind speeds. This control scheme is a simplified version that assumes a constant pitch value of 0° for wind speeds below rated power. For these speeds, the demanded generator torque (T_d) is equal to $T_d = K\Omega^2$ where K is a constant value of 0.97 and Ω is the generator speed. Some studies [3, 4] showed that varying K and the pitch angle below-rated power is useful to recover the energy loss due to LER. However, the K and pitch values were used in this study for all surface conditions to isolate the aerodynamic effect from the possible control scheme influence.

For the annual energy production (AEP) calculation, a Weibull distribution is used with a shape factor k of 2 and an average wind speed at the hub height of $7.2\,\mathrm{m\,s^{-1}}$.

2.3. CFD methodology

OpenFOAM 9.0 was used to perform 2D-RANS steady simulations using the SIMPLEC algorithm. In this regard, convergence is determined once a residual value lower than 1×10^{-6} is reached for every flow variable. Concerning the grid, a structured O-grid was used for a unit c with a radius of $40c$. As a result, the total number of cells is 1.4×10^5 with a first cell height of 1.12×10^{-6} to ensure y^+ values lower than 0.1.

The $k - \omega - SST$ turbulence model was chosen to model a fully-turbulent flow whereas the modeling of transitional flow was kept out of the assessment. Sørensen *et al.* [12] reported a limitation on the natural-transition prediction at high Re_c which could introduce inaccuracies in the assessment. Thus, clean polar curves were not computed in this study, and the clean power curve has been retrieved with experimental polar curves.

For the LER modeling, Wilcox's boundary condition (BC) [14] was used along with Hellsten's correction [13]. The non-dimensional equivalent sand grain k_s/c was set to 1.16×10^{-3} for the 30 % thick airfoils and 4.67×10^{-4} for the other two airfoils. The first value was demonstrated to be suitable in [15] whereas the second corresponds to the average sand grain height used in the experiments. Finally, the specific a_1 for each airfoil side was defined via the modification of the OpenFOAM source code, and the corresponding results are denoted as a_1 split method.

2.4. a_1 estimation

As a novel method, a specific value of a_1 was estimated per airfoil side with the corresponding notation of a_{1SS} and a_{1PS} for the suction side (SS) and the pressure side (PS), respectively. Figure 2a shows the blocks diagram of the methodology followed, the pressure coefficient C_p measurements of three airfoils, equipped with LER, is divided per each airfoil side to estimate a_1 locally by the minimization of the C_p root-mean-square error (RMSE) between measurements and 2D-RANS calculations, as shown by Figure 2b. The RMSE was employed in the literature for equivalent studies on other turbulent flows [18].

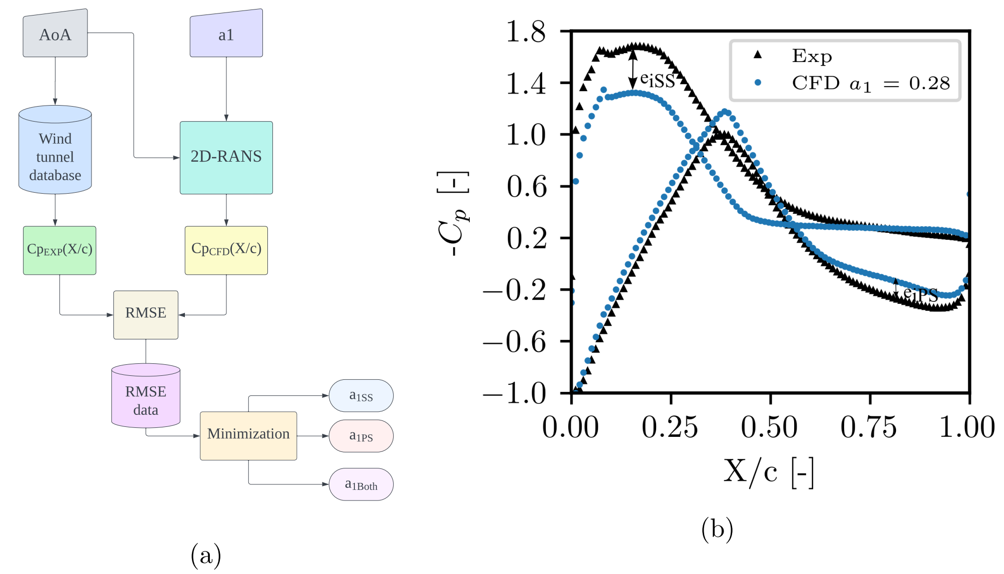

Figure 2: (a) Methodology for the estimation of a_1 per airfoil and AoA. (b) Error definition depending on the airfoil side for an i^{th} streamwise location.

As illustrated in Figure 2a, for a specific AoA and a_1 value, a 2D-RANS simulation was performed. Each simulation requires 28 min to reach 20 000 iterations in case 4 CPUs are used in its parallelization. This computational time challenges the use of automated algorithms to find an optimum a_1 value. Alternatively, a manual procedure was employed in this assessment based on two steps. First, the a_1 parameter was varied per AoA from 0.22 to 0.49. with a step of 0.01. Second, when a local minimum was located, the a_1 step was decreased to 0.005 for the two a_1 values adjacent to the minimum. This procedure was applied per each AoA ranging between $-20°$ and $20°$, with a step of 2°. This results in a total number of 735 simulations per airfoil.

Three options were studied to estimate a_1. Equations (1) and (2) compute the RMSE by taking the experimental C_p data on the airfoil SS or on the airfoil PS, respectively. Conversely, Equation (3) takes the C_p data of both airfoil sides. The first two equations are useful to assess the difference of a_1 on each airfoil side. In contrast, the latter equation is more similar to the current methodology followed in the literature and gives a compromise for the entire airfoil. The variable n in these equations means the number of points used to evaluate the C_p distributions and compute the corresponding difference via the use of B-spline interpolators. Convergence on the RMSE was found for a n value of 600.

$$\mathrm{RMSE}_{SS} = \sqrt{\frac{\sum_{i=0}^{n} e_{iSS}^2}{n}}; \tag{1}$$

$$\mathrm{RMSE}_{PS} = \sqrt{\frac{\sum_{i=0}^{n} e_{iPS}^2}{n}}; \tag{2}$$

$$\mathrm{RMSE}_{both} = \sqrt{\frac{\sum_{i=0}^{n} \left(e_{iSS}^2 + e_{iPS}^2\right)}{2n}}, \tag{3}$$

where $e_{iSS} = C_{piSSCFD} - C_{piSSexp}$ and $e_{iPS} = C_{piPSCFD} - C_{piPSexp}$.

3. Results

3.1. a_1 vs AoA

The need to adapt a_1 to the APG condition is justified by Figures 3a and 3b due to the non-linear variation of a_1 with the AoA depending on the SS or PS, respectively. In addition, a_1 is mostly lower than the default value of the $k-\omega-SST$ turbulence model of 0.31, ranging between 0.255 and 0.330, which highlights the need to decrease its value for APG flows. For all airfoils, a_1 is below 0.31 from an AoA of 8° for which C_{Lmax} is reached as confirmed by Figures 4a, 5a, 6a.

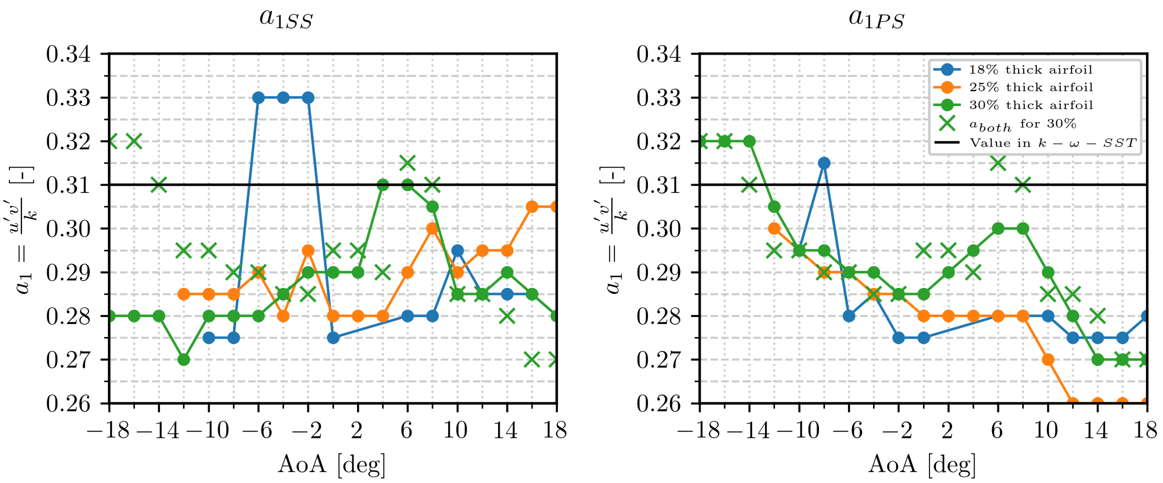

(a) (b)

Figure 3: Resulting a_{1SS} and a_{1PS} for the three airfoils in (a) and (b), respectively.

The coefficient a_{1both} is equivalent to the one considered by literature studies since they estimate it via the minimization of the aerodynamic coefficients error [6] or the C_p error [5]. However, the literature used a constant a_1 value for all the AoA range, whereas this study estimates a specific a_{1both} value per AoA. Figures 3a and 3b incorporate a_{1both} for the 30 % thick airfoil to quantify the difference with respect to a_{1SS} and a_{1PS}. Regarding the results, the difference in the a_1 value between the global, a_{1both} and local methods, i.e., a_{1SS} and a_{1PS}, is minimum for the a_{1PS} at negative AoAs. Hence, the C_p difference on the PS weighs more in the a_1 estimation for negative AoAs, which is in relation to the presence of flow separation on that airfoil side. In this regard, the opposite is found for the SS at positive AoAs because the C_p error weighs more on this side. The main benefit of splitting the a_1 value is found on the a_{1SS} since it provides the highest difference between the local and global methods. The main impact on the PS splitting is identified at 6° and 8°.

3.2. Airfoil performance

The overall prediction of the non-corrected RANS ($a_1 = 0.31$) is characterized by an overprediction of C_L beyond C_{Lmax} as well as an underprediction of C_D which turns into a higher C_L/C_D value than the other methods, as can be seen in Figures 4b, 5b and 6b. The error compensation in C_L/C_D can be identified in Table 1 where the relative error in aerodynamic coefficients is computed as $Error = (CFD - Exp.)/Exp.$ for an AoA of 6°. For all the airfoils, the non-corrected RANS provides lower relative error in C_L/C_D than the corrected-RANS. In addition, Figure 4a shows a significant mismatch in C_L between AoAs of $-8°$ and $2°$ which was confirmed with C_p distributions as an inaccuracy in predicting flow separation on the airfoil PS. In contrast, the f_b method substantially improves the prediction of C_L and C_D on the 30 % thick airfoil for negative AoAs. However, the f_b method prediction gets worse for positive AoAs which lowers the C_L/C_D with an error of -46.6 % at an AoA of 6°, as shown in Table 1. For the other two airfoils, the f_b method shows similar behavior as the default $k - \omega - SST$ model. Slight improvements can be identified as the prediction of C_{Lmax} in Figure 5a and the C_D value in Figure 6a.

	Error	**a1 = 0.31**	**f_b method**	**a1 split**
30% thick airfoil	ϵ_{C_L} [%]	-3.3	-18.1	-9.7
	ϵ_{C_D} [%]	29.3	53.4	24.9
	ϵ_{C_L/C_D} [%]	-25.2	-46.6	-27.7
25% thick airfoil	ϵ_{C_L} [%]	8.6	5.4	-0.5
	ϵ_{C_D} [%]	22.1	23.5	26.9
	ϵ_{C_L/C_D} [%]	-11.2	-14.8	-21.7
18% thick airfoil	ϵ_{C_L} [%]	7.1	9.1	2.6
	ϵ_{C_D} [%]	11.4	0.6	9.4
	ϵ_{C_L/C_D} [%]	-3.9	8.5	-6.2

Table 1: Relative error of C_L, C_D and C_L/C_D computed as $Error = (CFD - Exp.)/Exp.$ for $AoA = 6°$.

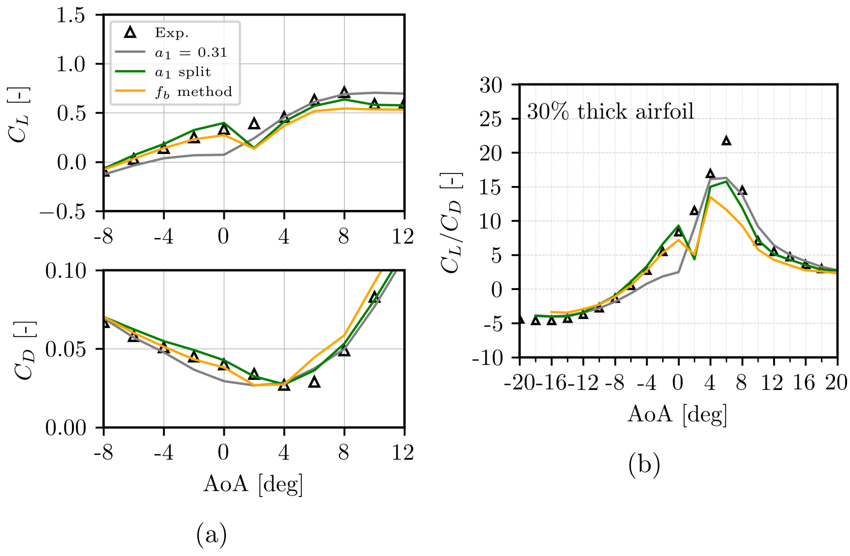

Figure 4: (a) C_L and C_D vs AoA. (b) C_L/C_D vs AoA. Results for the 30 % thick airfoil.

Alternatively, the a_1 split method substantially improves the C_L prediction for the three airfoils, especially for the thinnest airfoils. The error ϵ_{C_L} in Table 1 for the a_1 split method is $-0.5\,\%$ whereas it is $8.6\,\%$ for the $a_1 = 0.31$ solution and $5.4\,\%$ for the f_b method. Additionally, the overall C_L improvement can be identified in Figure 5a by a suitable prediction of the linear C_L region, the C_{Lmax} value, and the post-stall trend. However, the C_L mismatch deserves special mention at an AoA of $2°$ in Figure 4a for which all the simulations fail. This may be related to the steady assumption followed in the simulations which may differ from the experimental one. Finally, a C_D error is shared for all airfoils which deviates the predicted C_L/C_D from the experimental one.

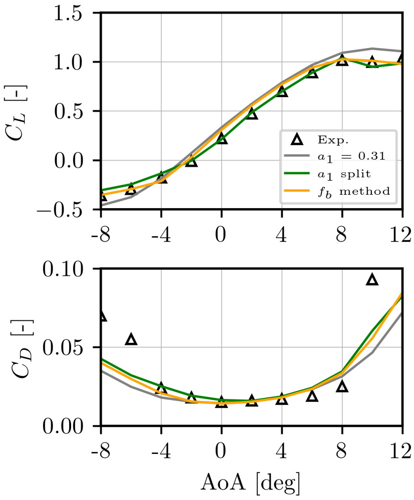

(a)

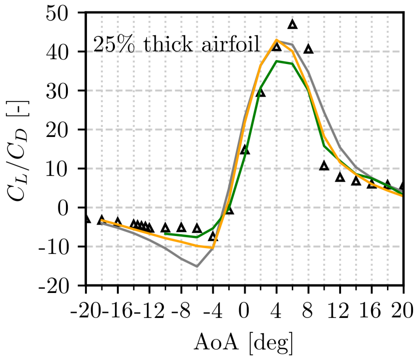

(b)

Figure 5: (a) C_L and C_D vs AoA. (b) C_L/C_D vs AoA. Results for the 25 % thick airfoil.

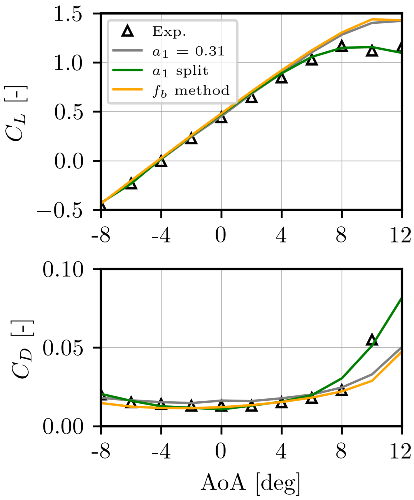

(a)

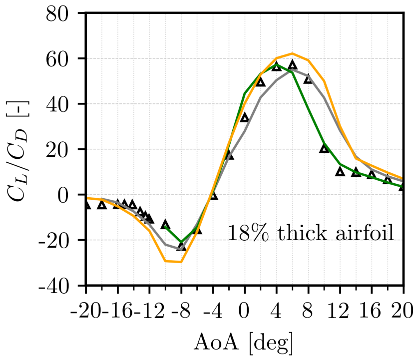

(b)

Figure 6: (a) C_L and C_D vs AoA. (b) C_L/C_D vs AoA. Results for the 18 % thick airfoil.

3.3. Wind-turbine performance

Comparing the power prediction of *Exp. Clean* and *Exp. Rough* in Figure 7a, LER causes a drop in power which translates to an AEP loss of 20.8 %. While this AEP loss is higher than the one reported in other studies [21, 22, 23], the blade thickness in this study is relatively higher resulting in a significant weight of the 30 % aerodynamic data on the wind turbine performance. Concerning Timmer and Bak [24], the loss in power caused by LER can be mainly explained by the lowering of C_L and increase of C_D which lowers the driving force coefficient C_x, defined by Equation 4, where ϕ is the flow angle. As a result, loads are decreased by LER as Figure 7b shows.

$$C_x = C_L \left(sin\ \phi - \frac{1}{C_L/C_D} cos\ \phi \right) \tag{4}$$

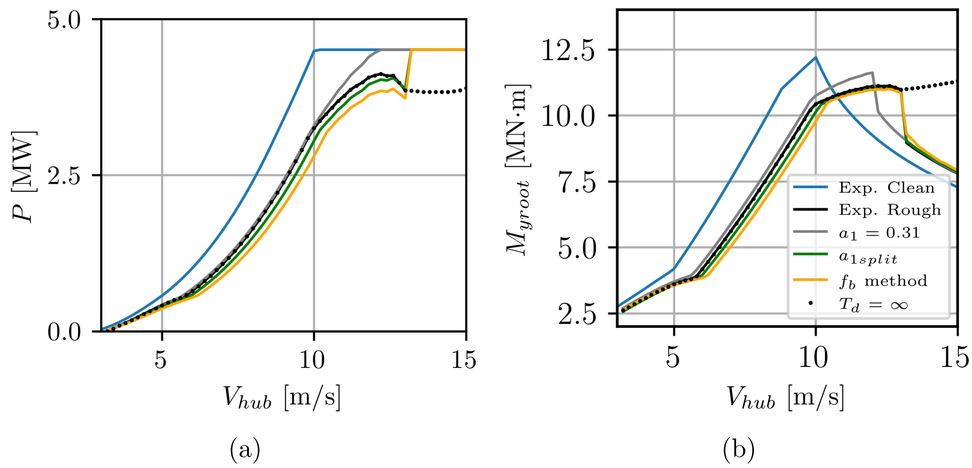

Figure 7: (a) Power curve. (b) Distribution of flap-wise bending moment at blade root.

However, the drop in power for *Exp. Rough* deserves special mention between 12 m s^{-1} and 13 m s^{-1} as well as the sudden increase in power between 13 m s^{-1} and 13.2 m s^{-1}. Figure 8 shows the pitch and demanded torque T_d of the wind turbine as well as the AoA and C_x value at a z_b of 70 % L. Regarding the *Exp. Rough*, the T_d value is far from the nominal value so the pitch system is keeping the pitch value at 0°, and in turn, the AoA continues to increase. At 12 m s^{-1} the AoA reaches a value of 8° defining the C_{Lmax} condition of Figures 4a, 5a and 6a and further increases for higher wind speeds at the hub height V_{hub}. Thus, the blade suffers from flow separation from 12 m s^{-1}, which results in the mentioned power drop. However, from 13 m s^{-1}, the overall torque of the blade is enough to reach the nominal T_d value and the controller finds a pitch condition to fulfill the specified-nominal T_d and suddenly pitches the blade from 6° which reduces the AoA, avoids flow separation, increases C_x and ensures rated power. In case the nominal T_d value is specified to an excessive value ($T_d = \infty$), the control schema does not enable the pitch actuator, and the pitch value remains at 0° which causes the blade to continue under flow separation conditions making the power-curve shape to be similar to the one of a stalled-regulated wind-turbine.

Regarding the simulations, between 4 and 10 m s^{-1}, the non-corrected RANS ($a_1 = 0.31$) is providing a power loss similar to *Exp. Rough*, whereas the corrected RANS is causing a higher loss. This is due to the error compensation in C_L/C_D ratio for the non-corrected RANS solution previously commented, which is not showing a physical representation. Hence, the inaccuracy of the non-corrected RANS in predicting flow separation implies a relatively higher C_L/C_D and

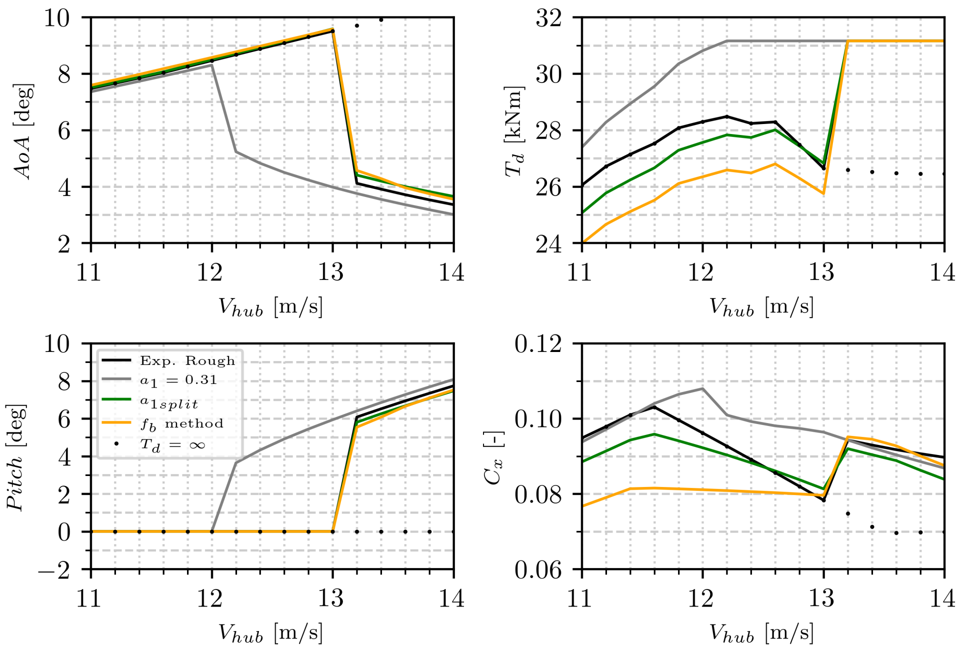

Figure 8: Operational assessment for wind speeds near rated power. While AoA and C_x, are extracted for the corresponding-blade location $Z_b = 70\,\%\ L$, Pitch and T_d, are overall wind-turbine parameters.

C_x which results in a sooner action of the pitch system from $12.2\,\mathrm{m\,s^{-1}}$ for which rated power is reached. As a result, the LER effects are underestimated with respect to *Exp. Rough* which turns into an error on AEP loss of 2.5 %. Besides, an overshoot of the flap-wise bending moment at blade root M_{yroot} is found in Figure 7b near rated power.

In contrast, the corrected RANS provides a coherent shape of the power curve and the M_{yroot} distribution. Figure 8 shows that the modeling of flow separation is causing a lower C_x value and the pitch system behaves similarly to the case of *Exp. Rough* making the blade enter in flow separation whereas it was not the case for the non-corrected RANS case. Nevertheless, there is an offset in power below the rated wind speed between the corrected RANS and *Exp. Rough* which is higher in the f_b method than in the a_1 split method resulting in errors in AEP loss of $-7.7\,\%$ and $-3.6\,\%$. This is justified by the already mentioned error in C_L/C_D and the resulting lowering in C_x which can be seen in Figures 5b and 4b and Table 1.

4. Conclusions

A novel approach has been followed to estimate a_1 per airfoil side and AoA due to the literature statement about its dependency on the APG condition which will be different for each airfoil side and AoA. C_p experimental data under LER conditions of three airfoils with relative thicknesses of $30\,\%c$, $25\,\%c$ and $18\,\%c$ were used for the estimation. Additionally, the resulting prediction in aerodynamic coefficients and wind-turbine performance was compared with the default value of $a_1 = 0.31$ and the f_b method.

This study presents novel findings on the relationship between a_1 and the local-APG condition in airfoil flows. The non-linear variation of a_1 with respect to the AoA is unique to each airfoil and airfoil side. Hence, each side offered a different APG and, in turn, a different a_1. In the three studied airfoils, there is a change in the a_1 trend at the AoA where C_{Lmax} is reached. The use of splitting the a_1 value has been demonstrated for the first time in the literature as a valid option and has shown significant improvements in aerodynamic coefficient predictions with a maximum error reduction of 8.1 %, as shown in Table 1. Thus, the results of this study have shown the importance of including a dependency of a_1 with the APG condition in future formulations of the $k - \omega - SST$ turbulence model. Regarding the f_b method, this study has extended its use to LER conditions and demonstrated significant improvements in some of the AoAs and airfoils. However, the a_1 split methodology resulted in a lower error for a greater range of angles of attack across all airfoils compared to the f_b method.

Finally, this study quantifies the failure of the non-corrected RANS solution in predicting the wind-turbine performance. On the one hand, the modelling of LER in wind turbine performance is concluded to be valid as the non-corrected RANS matches the performance of the *Exp. Rough* up to wind speeds of $10\,\mathrm{m\,s^{-1}}$. However, there is a substantial failure near rated wind-speed which is concluded to be related to the scarce prediction of flow separation at AoAs greater than 8°. On the other hand, the corrected-RANS solution replicated the shape of the power and M_{yroot} curves with an offset in value due to a C_D error which was also implicit in the non-corrected-RANS solution. Nevertheless, the numerical solution of the corrected-mean flow could be used in the future for extracting BL properties for noise estimations or add-on sizing thankfully to the verification performed by this study.

Even though this study's data was not enough to find a general a_1 expression, the employed methodology can be useful for searching a robust a_1 formulation after employing extensive research for other APG conditions.

5. References

[1] Manolesos M, Sørensen N N, Troldborg N, Florentie L, Papadakis G, Voutsinas S 2016 *J. Phys.: Conf. Ser.* **753** 022014
[2] Kamruzzaman M, Bekiropoulos D, Wolf A, Lutz Th, Krämer E 2014 *20th AIAA/CEAS Aeroacoustics Conference*
[3] Gutiérrez R, Llorente E, Ragni D 2022 *J. Phys.: Conf. Ser.* **2151** 012001
[4] Kelly J, Vogel C, Willden R 2021 *Wind Energy* **25**
[5] Matyushenko, A A and Garbaruk, A V 2016 *J. Phys.: Conf. Ser.* **769** 012082
[6] Campobasso S M, Castorrini A, Cappugi L, Bonfiglioli A 2022. *Wind Energy* **25**
[7] Simpson, R 1987 *AIAA Journal* **25**
[8] Bangga, G et al. 2018. *J. Phys.: Conf. Ser.* **974** 012019
[9] Gutierrez R, Zamponi R, Ragni D, Llorente E, Aranguren P 2023 *Wind Energy* **26**
[10] Bir G S 2006 *User's Guide to PreComp* (National Renewable Energy Laboratory (U.S.))
[11] Bossanyi E A 2003 *Bladed Theory Manual* (Garrad Hassan & Partners Ltd)
[12] Sørensen N N *et al.* 2016 *J. Phys.: Conf. Ser.* **753**
[13] Hellsten A and Laine S 1997 *22nd Atmospheric Flight Mechanics Conference*
[14] Wilcox D C 2006 *Turbulence Modeling for CFD. 3rd Edition* (DCW Industries)
[15] Gutiérrez R, Llorente E, Ragni D, Aranguren P 2022 *J. Phys.: Conf. Ser.* **144**
[16] Gutiérrez R, Llorente E, Echeverria F, Ragni D 2020 *J. Phys.: Conf. Ser.* **1618**
[17] Llorente E, Gorostidi A, Jacobs M, Timmer W A, Munduate X, Pires O 2014 *J. Phys.: Conf. Ser.* **524**
[18] Romanova D et al. 2022 *Fluids* **7**
[19] Jonkman J, Butterfield S, Musial W, Scott G 2009 *Definition of a 5-MW Reference Wind Turbine for Offshore System Development* (National Renewable Energy Lab. (NREL))
[20] Popko W *et al.* 2018 *IWES Wind Turbine IWT-7.5-164. Rev 4* (Fraunhofer Institute for Wind Energy Systems IWES)
[21] Langel M C et al. 2015 *AIAA 33rd Wind Energy Symposium*
[22] Papi F, Ferrara G, Bianchini A 2020 *J. Phys.: Conf. Ser.* **1618**
[23] Campobasso S M, Castorrini A, Ortalani A, Minisci E 2023 *Renewable and Sustainable Energy Reviews* **178**
[24] Timmer W A and Bak C 2013 *Advances in Wind Turbine Blade Design and Materials* (Woodhead Publishing)
[25] Grasso F 2021 *Handbook of Wind Energy Aerodynamics* (Springer)